Exp Fluids (2011) 51:313–326
DOI 10.1007/s00348-011-1049-7

RESEARCH ARTICLE

Turbulence in rough-wall boundary layers: universality issues

Mohammad Amir · Ian P. Castro

Received: 8 September 2010 / Revised: 15 December 2010 / Accepted: 28 January 2011 / Published online: 15 February 2011

Abstract Wind tunnel measurements of turbulent boundary layers over three-dimensional rough surfaces have been carried out to determine the critical roughness height beyond which the roughness affects the turbulence characteristics of the entire boundary layer. Experiments were performed on three types of surfaces, consisting of an urban type surface with square random height elements, a diamond-pattern wire mesh and a sand-paper type grit. The measurements were carried out over a momentum thickness Reynolds number (Re_θ) range of 1,300–28,000 using two-component Laser Doppler anemometry (LDA) and hot-wire anemometry (HWA). A wide range of the ratio of roughness element height h to boundary layer thickness δ was covered ($0.04 \leq h/\delta \leq 0.40$). The results confirm that the mean profiles for all the surfaces collapse well in velocity defect form up to surprisingly large values of h/δ, perhaps as large as 0.2, but with a somewhat larger outer layer wake strength than for smooth-wall flows, as previously found. At lower h/δ, at least up to 0.15, the Reynolds stresses for all surfaces show good agreement throughout the boundary layer, collapsing with smooth-wall results outside the near-wall region. With increasing h/δ, however, the turbulence above the near-wall region is gradually modified until the entire flow is affected. Quadrant analysis confirms that changes in the rough-wall boundary layers certainly exist but are confined to the near-wall region at low h/δ; for h/δ beyond about 0.2 the quadrant events show that the structural changes extend throughout much of the boundary layer. Taken together, the data suggest that above $h/\delta \approx 0.15$, the details of the roughness have a weak effect on how quickly (with rising h/δ) the turbulence structure in the outer flow ceases to conform to the classical boundary layer behaviour. The present results provide support for Townsend's wall similarity hypothesis at low h/δ and also suggest that a single critical roughness height beyond which it fails does not exist. For fully rough flows, the data also confirm that mean flow and turbulence quantities are essentially independent of Re_θ; all the Reynolds stresses match those of smooth-wall flows at very high Re_θ. Nonetheless, there is a noticeable increase in stress contributions from strong sweep events in the near-wall region, even at quite low h/δ.

M. Amir · I. P. Castro (✉)
School of Engineering Sciences, University of Southampton, Highfield, Southampton SO17 1BJ, UK
e-mail: i.castro@soton.ac.uk

Present Address:
M. Amir
Department of Engineering, University of Aberdeen, Aberdeen AB24 3FX, UK

1 Introduction

Turbulent flows over smooth surfaces have been studied extensively for a long time, both experimentally and theoretically. The importance of the wall layer was convincingly demonstrated experimentally by Kline et al. (1967). Despite its significant importance in industrial applications, much less is known for flows over rough surfaces. Surface roughness is a defining feature of many of the high Reynolds number flows found in engineering. In fact, the higher the Reynolds number, the more likely are significant effects of roughness, since the size of the roughness elements becomes increasingly large compared to the near-surface viscous length appropriate for smooth-wall flows. As a result, turbulent boundary layers over the hulls of ships and submarines, within turbo-machinery, and over the surface of the earth are all cases for which the smooth-wall idealization rarely applies. Unfortunately, the impact

of surface roughness is not entirely understood, and a number of important fundamental questions have not yet received a satisfactory answer. For this reason, wall-bounded shear flows with roughness have been the focus of a large body of research. Reviews of much of this work are given by Raupach et al. (1991) and Jiménez (2004). The conclusion of both reviews based on a majority of both the experimental and computational evidence is that the flow structure is unaffected by surface roughness in the outer region of the shear layer. This supports the wall similarity hypothesis of Townsend (1976), which states that the turbulence structure is unaffected by the surface condition at a sufficient distance from the wall. This distance is generally thought to be 3–5 roughness heights (h) from the wall (Raupach et al. 1991; Flack et al. 2005). The underlying assumptions of Townsend's hypothesis are that the Reynolds number is sufficiently high and that h is small compared to the boundary layer thickness.

Since Raupach et al.s (1991) review, the concept of wall similarity has come into question. Experimental studies of rough-wall boundary layers by Krogstad et al. (1992), Krogstad and Antonia (1999), Tachie et al. (2000), Keirsbulck et al. (2002) and Volino et al. (2009) have all observed significant changes to the Reynolds stresses that extend well into the outer layer for flows over (three-dimensional) woven mesh and transverse (two-dimensional) bar roughness. Numerical simulations of turbulent channel flow by Leonardi et al. (2003) and Bhaganagar et al. (2004) also show that roughness effects can be observed in the outer layer. However, the experimental studies of Kunkel and Marusic (2006) and Flack et al. (2005) provide support for wall similarity in rough-wall boundary layers in terms of both the mean flow and the Reynolds stresses. The work of the former is notable because of the extremely high Reynolds number and large separation of scales in the turbulent boundary layers that were studied.

Jiménez (2004) emphasized the obvious point that the conflicting views regarding the validity of the wall similarity hypothesis may be due to the effect of the relative roughness, h/δ, on the flow (where δ is the boundary layer thickness). He concluded that if the roughness height is small compared to the boundary layer thickness ($h/\delta < 1/50$), the effect of the roughness should be confined to the inner layer and wall similarity will hold. If, on the other hand, the roughness height is large compared to the boundary layer thickness ($h/\delta \geq 1/50$), roughness effects on the turbulence may extend across the entire boundary layer, and the concept of wall similarity will be invalid. But some of the work mentioned above contradicts this conclusion in one respect or another.

There is thus considerable current debate about the structure of rough-wall flows and exactly how and under what circumstances the roughness effects extend throughout the flow. Even if one accepts that provided $h/\delta < 0.02$, say, Townsend's hypothesis is valid, it has never been determined just how large h/δ must be before it becomes untenable, as it eventually must. And does the critical value of h/δ, $(h/\delta)_c$ say, depend on the geometrical characteristics of the roughness? Furthermore, once $(h/\delta)_c$ has been exceeded, how does the structure of the boundary layer differ from that of the more 'classical' (smooth or 'small-roughness') flow and to what extent do the differences depend on the topology of the roughness? Of course, once h/δ becomes of O(1), one could consider the flow (initially) simply as a free stream over a collection of bluff bodies and one then certainly expects at least some features of the flow structure to depend on the specific surface topology. But as the flow develops over a longer and longer fetch of the same roughness, the boundary layer grows, so that h/δ gradually falls and eventually (presumably) the classical situation will emerge. Does the particular h/δ at which this first happens depend on the flow history prior to the start of the rough surface?

In our earlier paper (Castro 2007), it was shown that the classical two-parameter profile can be used to collapse mean velocity data up to surprisingly large values of h/δ—at least 0.2—for a wide range of typical three-dimensional roughness types. There was evidence, however, that the turbulence characteristics changed for rather lower values. Flack et al. (2007) examined the effect of increasing roughness height on the outer layer turbulent statistics in fully developed turbulent boundary layers on two types of three-dimensional rough surfaces. They concluded that not only the mean flow but also the turbulence remained essentially unaffected by the roughness. However, the highest value of h/δ obtained in their study was only 0.052 which although higher than Jiménez's criterion is still quite small.

The purpose of the present paper is to address the issues discussed above, particularly those concerning the turbulence characteristics and how they are affected by increasing h/δ. We describe experiments on a number of rough surfaces and i) examine the roughness effects on the mean flow and turbulence throughout the boundary layer, ii) identify to what extent these are different in both the near-wall region and the outer flow from those typical of classical smooth-wall flows, iii) determine $(h/\delta)_c$, iv) ascertain whether this value depends on the nature of the 3D roughness, and (v) identify what are the most significant structural differences throughout the boundary layer once $h/\delta > (h/\delta)_c$ and how these subsequently vary with increasing h/δ.

In the following section, we summarize major features of the classical mean flow scaling and discuss the crucial issue of determining wall stress, before describing the experimental methodology in Sect. 3. Basic mean flow and turbulence data are presented and discussed in Sects. 4 and 5, respectively. Further, structural data from quadrant

analysis are discussed in Sect. 6 before conclusions are summarized in Sect. 7.

2 Mean flow scaling

In classical turbulence theory, the turbulent boundary layer is considered to consist of an inner and outer layer which only interacts in a limited sense. This has led to a tradition of regarding the surface geometry as a boundary condition which only affects the velocity distribution in the roughness region (often called the roughness sublayer). This layer extends only a few roughness heights away from the wall (e.g. Rotta 1962). The effect of surface roughness on the boundary layer mean velocity profile is classically expressed using a roughness function ΔU^+, which modifies the usual smooth-wall formulation, as expressed below for the fully rough case,

$$U^+ \equiv \frac{U}{u_\tau} = \frac{1}{\kappa}\ln(y-d)^+ + B - \Delta U^+ + w\left(\frac{y}{\delta}\right) \quad (1)$$

where u_τ is the friction velocity ($\sqrt{\tau_w/\rho}$), $B = 5.2$ and $\kappa = 0.41$, as determined for smooth-wall surfaces, $w\left(\frac{y}{\delta}\right)$ is the outer layer wake function, and d is the zero plane displacement. Meteorologists have always used a log law of the form

$$U^+ = \frac{1}{\kappa}\ln\left(\frac{y-d}{y_o}\right). \quad (2)$$

For a smooth wall, d would be zero and for a rough wall, with y measured from the bottom of the roughness elements, d can be interpreted as the effective height of momentum extraction (i.e. where the surface drag is 'seen' to act by the flow aloft, Jackson 1981) and is always less than h. y_o is the roughness length and is typically $0.1h$ but this depends significantly on the roughness geometry. For fully rough surfaces (i.e. where viscous effects do not contribute noticeably to the surface drag), Castro (2007) argued that this is the more appropriate form of the log law, since it contains no viscous length scale (ν/u_τ), and such flows are essentially independent of Re_θ, the momentum thickness Reynolds number, being dependent instead (in principle at least) on θ/y_o.

The assumption of an outer layer unaffected by the wall condition implies that the velocity defect function

$$U_e^+ - U = -\frac{1}{\kappa}\ln\left(\frac{(y-d)}{\delta}\right) + \frac{\Pi}{\kappa}\left[2 - w\left(\frac{(y-d)}{\delta}\right)\right] \quad (3)$$

must be the same for rough and smooth walls. U_e is the free-stream velocity (reached at $y - d = \delta$) and $w(0) = 0$, $w(1) = 2$ and $\int_0^\infty w\mathrm{d}(\frac{(y-d)}{\delta}) = 1$ provide the normalization conditions for the wake function. Π is the wake strength parameter. The similarity in the mean velocity in the outer layer can therefore be assessed using velocity-defect scaling and, as mentioned above, it was shown earlier that mean velocity profiles remain self-similar to surprisingly large values of h/δ, whatever the nature of the (three-dimensional) surface topology (Castro 2007), although Π rises slowly with decreasing θ/y_o.

Assessing the similarity of both mean flow and turbulence profiles requires determination of the wall-shear stress (to obtain u_τ). This is not easy even for smooth walls, but is much more difficult on rough ones, except in fully developed internal flows where the total surface stress is related directly to the (easily measurable) axial pressure gradient. In boundary layers, the wall stress is typically deduced from either near-wall measurements of the turbulence shear stress, $-\overline{uv}$, where lower case quantities refer as usual to the instantaneous fluctuating components of velocity, or the evaluation of velocity profiles in terms of a Clauser chart, or an equivalent full profile formulation. The latter requires assumptions about the form of the wake profile, and it has been pointed out that the Clauser chart method could, at least for smooth walls, potentially mask subtle Reynolds number-dependent behaviour (Wei et al. 2005). Connelly et al. (2006) determined u_τ for their rough surfaces by using a procedure based on the modified Clauser chart method proposed by Perry and Li (1990), with values confirmed using the total stress method, which assumes a constant stress region equal to the wall shear stress that exists in the overlap and inner region of the boundary layer. The results from the modified Clauser chart and the total stress methods agreed to within 5% for their rough surfaces. In the present study, the total stress method was employed to determine u_τ; for these fully rough surfaces, this amounts to using the measured (average) value of $-\overline{uv}$ in the inertial sublayer. There are inevitable uncertainties, not least in that, for some surfaces, measurements have suggested that this underestimates the wall stress (see Cheng and Castro 2002), but this was deemed better than the much more uncertain approach of trying to deduce all the unknowns from the mean velocity profile alone. The most widely used approach for determining both d (and then y_o) is first to obtain the value of u_τ independently—e.g. from the $\overline{uv}$ profile as in the present work or, ideally, from accurate surface drag balance data. This u_τ can then be used as the required slope to fit the mean velocity data to the usual logarithmic law, choosing the d that yields the best fit. This was the method used in the present work.

3 Experimental arrangements

The experiments were conducted in a nominally zero-pressure gradient boundary layer within a blow-down wind

tunnel at the University of Southampton. The tunnel has a working section about 4.5 m in length and 0.9 m × 0.6 m in area, with a tunnel velocity range of 0–30 ms^{-1}. The free-stream turbulence intensity in the tunnel is ≈0.25%. The floor was completely covered with three different types of roughness. The first surface was an urban type roughness which comprised 5-mm-square cuboids having five different heights chosen from a normal distribution with a mean and standard deviation of 5 and 1.5 mm, respectively. These elements were arranged in a staggered pattern, and the size of the repeating unit of this surface was 40 by 40 mm (giving 16 elements in each such unit). This ensured that the total element volume, as a percentage of the product of the repeating unit area and the mean element height, was identical to the surfaces used by Cheng and Castro (2002), hereafter denoted by CC. This work therefore compliments the earlier study reported in the latter, where full details of the surface which here we call the 'block' roughness, can be found. Figure 1 shows a schematic plan view and a 3D view of a single 'repeating unit' of this block roughness. The vertical profile locations are indicated by dots. Because of the spatially inhomogeneous nature of the flow in the roughness sublayer, to obtain representative spatially averaged turbulence properties within this layer, it is in principle necessary to average a sufficiently large number of individual point measurements. CC therefore took 64 profiles over a single repeating unit, at the locations indicated by the dots in Fig. 1. In the current work, only one location was chosen (labelled 'measurement location' in Fig. 1). The selection of this location was made using the data of CC by comparing the Reynolds-stress profiles obtained by spatially averaging all 64 vertical profiles with each of the individual profiles. The location at which an individual profile most closely matched the spatially averaged profile was chosen to be the measurement location for the current experiments. This avoided the necessity of obtaining multiple profiles within the roughness sublayer.

The second surface consisted of a regular diamond-patterned wire mesh, not too dissimilar to that used by Krogstad and Antonia (1999) (although theirs was square-patterned) and identical to that used in the more recent channel experiments of Birch and Morrison (2010). The mesh wavelength was 28.6 and 9.7 mm in the spanwise and axial directions, respectively, with a total mesh depth of about 4 mm (Fig. 2a). Vertical profile data were obtained along a line above the geometrical centre of the diamond. The third surface was a grit-type roughness, again identical with a surface used by Birch and Morrison (2010); this was a 16-gauge industrial open-type silicon carbide abrasive sheet with a sparse and isotropic grit pattern having a highly non-Gaussian distribution (Fig. 2b). The total grit depth was about 2 mm from the base of the grit particles. For both these surfaces, measurements did not extend much into the roughness sublayer, and profile fits were limited to the region above that layer (and, of course) below the outer wake region.

In every case, the roughness was mounted on 10-mm-thick baseboards which were placed on the floor of the working section. A leading edge ramp some 200 mm long was positioned at the front of the first roughness board to sweep the thin contraction-exit boundary layer up to the top of these baseboards. Some experiments were also conducted on the smooth bottom surface of the working section, for reference purposes. Mean and fluctuating velocities, denoted as (U, V) and (u, v) respectively, were measured using standard crossed-hot-wire anemometry (HWA) and Laser Doppler anemometry (LDA). For the HWA, signals from University of Newcastle (NSW) bridges were filtered and digitized *via* a 16-bit A/D

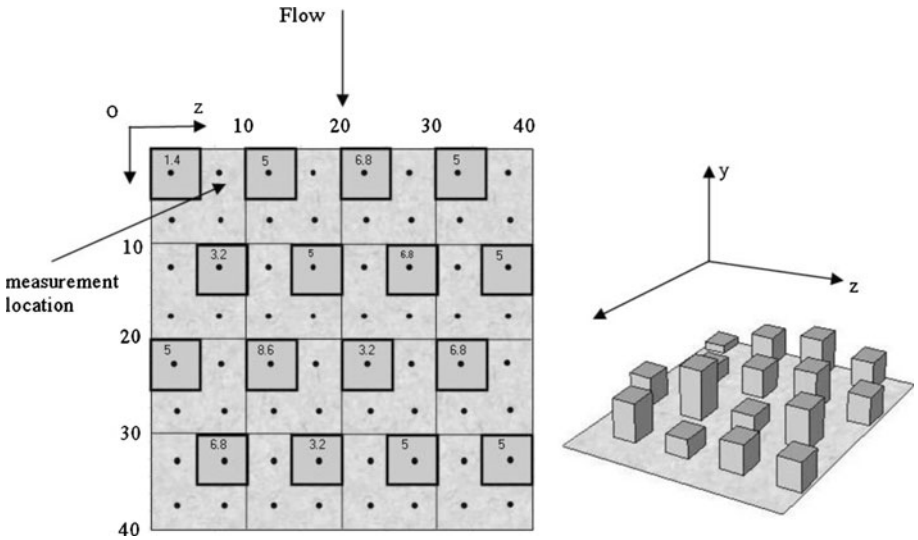

Fig. 1 Schematic plan view and 3D view of a single repeating unit of the block surface. Dimensions in mm, with element heights indicated on the plan view

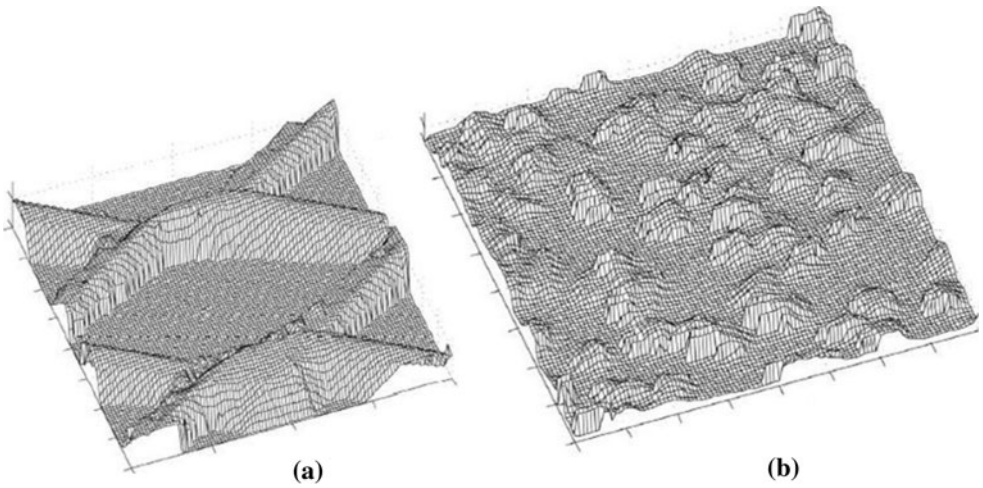

Fig. 2 Mesh roughness (**a**), with a total depth of 4 mm, and grit roughness (**b**), with a total depth of 2 mm. The images are from laser profilometer scans, from Birch and Morrison (2010)

converter (IOTEech ADC488/8SA), which was operated using virtual instruments (VI) written in LabView (from National Instruments) mounted on a PC. The VI package was developed and maintained by the EnFlo laboratory at the University of Surrey.

Hot-wire probes were gold-plated tungsten wires with an active length of about 1 mm, and the X-wires were nominally ±60° to the mean flow direction, to minimize errors arising from the finite yaw response. These have been shown to be significant with standard 45° wires (e.g. Perry et al. 1987; Krogstad et al. 1992). Yaw calibrations using the effective cosine law (typically over probe yaw angles up to ±30°) were performed in the free stream against a standard Pitot-static tube using a micromanometer whose output was passed to the same A/D system. Corrections were also made to the near-wall turbulence stress measurements to account for the high-turbulence intensities (using Tutu and Chevray's 1975, results). Sampling rates were typically between 5 and 10 kHz, with sampling times of 60–120 s. The probes were mounted on a 2D traverse system, driven by the same software that obtained the probe data (whether HWA or LDA).

As a check on the adequacy of the hot-wire data, additional measurements were also made using LDA. The data were obtained using a two-component (Dantec Burstware) system operated with an argon-ion laser run at 2 W. A fibre optic probe containing a 300-mm focal length lens was located outside the wind tunnel. A beam expander was mounted on this probe to allow measurements to be taken at the centreline of the wind tunnel. The Burst Spectrum Analysers were run in coincidence mode, and typically, 40,000–60,000 validated bursts were recorded during sampling times of 60–180 s and sampling rates up to 1 kHz. Transit time weighting was used on all statistical averaging to minimize bias errors. As demonstrated later, mean and turbulence profile data obtained from these two techniques agreed very well.

The free-stream velocity was varied between 5 and 20 ms^{-1} and, for each profile, was measured using a Pitot-static tube mounted at the same axial location; the same probe was used for the hot-wire calibrations. Any profile which showed a hot-wire free-stream velocity drift of more than 1% was rejected. For all the test cases, the mean velocity profiles were obtained at various locations downstream of the leading edge of the roughness. This led to wide ranges of momentum thickness Reynolds number ($1{,}300 < Re_\theta < 28{,}000$) and roughness element height to boundary layer thicknesses ($0.04 < h/\delta < 0.40$). The boundary layer thickness at each of the measurement locations was defined as the height at which the velocity was 99% of the free-stream velocity, U_e.

4 The mean flow

The mean velocity profiles in wall coordinates for the three rough surfaces at $Re_\theta \approx 11{,}000$ are shown in Fig. 3. Smooth wall results from Fernholz and Finley (1996) are shown for comparison. The data for the block and mesh surface were obtained using LDA, whereas for the grit surface data, HWA was used. The relative roughness heights at the measurement locations were $h/\delta = 0.043$, 0.035 and 0.033 for the block, mesh and grit surfaces, respectively. The results for Krogstad and Antonia's (1999) mesh surface and CC's staggered array of uniform cubes, both obtained using HWA, are included in the figure. All the rough surfaces display the usual linear log region, shifted below the smooth profile by the roughness function ΔU^+, indicating an increased momentum deficit on these surfaces. The roughness function can be expressed as $\Delta U^+ = A + \frac{1}{\kappa}\ln(Re_\tau)$ where $Re_\tau = y_o u_\tau / \nu$ (by equating the log-law part of Eq. 1 with Eq. 3) and the legend contents in Fig. 3 are listed in order of decreasing θ/y_o, equivalent to

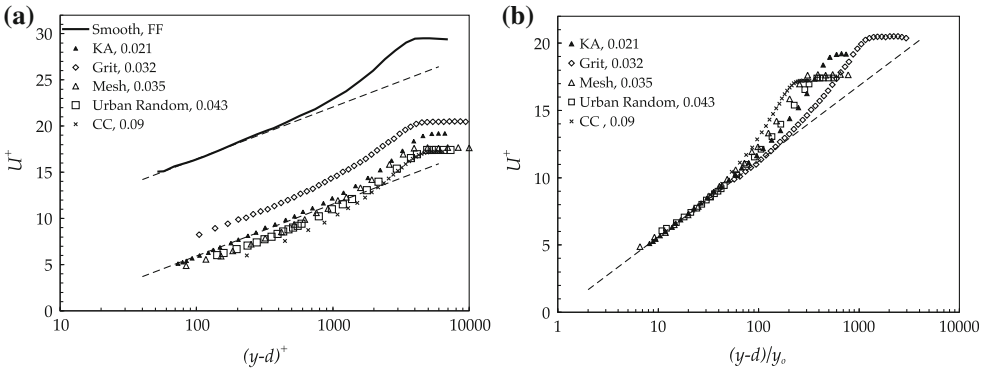

Fig. 3 Mean velocity profiles. **a** for $Re_\theta \approx 11{,}000$, viscous scaling; **b** y_o scaling. The legends include values of h/δ for each case and, from top to bottom, are in order of decreasing θ/y_o and thus increasing roughness Reynolds number, $Re_\tau = y_o u_\tau/\nu$. *Dashed lines* show the usual log law, with the *lower line* in (**a**) shifted by $\Delta U^+ = 10.5$

Table 1 Salient parameters for the data shown in Fig. 3

Surface	Symbol	h/δ	θ/y_o	Re_τ	ΔU^+	y_o/h
Grit	◇	0.033	148.3	3.53	8.3	0.027
KA mesh	▲	0.021	67.3	8.9	10.5	0.083
Mesh	△	0.035	43.8	12.7	11.4	0.095
Random blocks	□	0.066	49.8	13.0	11.5	0.066
CC cubes	×	0.047	33.4	19.9	12.6	0.047

KA refers to Krogstad and Antonia (1999) and CC to Cheng and Castro (2002)

increasing Re_τ and ΔU^+. Table 1 lists the salient parameters for these particular cases. As expected, a trend of increasing ΔU^+ with increasing roughness Reynolds number (and decreasing θ/y_o) is observed. Note that the parameters θ/y_o and ΔU^+ do not vary monotonically with h/δ, so the latter is only a crude measure of the 'strength' of the roughness. Figure 3b shows the data plotted using the more appropriate y_o scaling, and Table 1 includes the values of y_o/h for each case. Again, note that these do not vary monotonically with the controlling parameter θ/y_o, which emphasizes the extent to which the specific roughness geometry determines y_o/h. Note also that, in conformity with Castro (2007), this figure suggests a small increase in the strength of the wake with decreasing θ/y_o : Π (proportional to the maximum difference between the log law and the wake profile) is noticeably larger for the CC data than for the grit data.

Despite the small differences in the wake component, data plotted in defect form show reasonably good collapse, as demonstrated in Fig. 4a, which shows the data of Fig. 3 ($Re_\theta \approx 11{,}000$). Clauser's scaling parameter $\Delta = \delta^* U_e/u_\tau$, where δ^* is the displacement thickness, is used to normalize the wall distance as this is more appropriate than the boundary layer thickness. Krogstad and Antonia's (1999) mesh data are included and are largely indistinguishable from the present results. To demonstrate the level of agreement between LDA and HWA, the block surface data obtained using the latter are also included. Recall that all these data are for $Re_\theta \approx 11{,}000$, but very similar results were found over a wide range of Re_θ.

Figure 4b emphasizes the expected collapse independent of Re_θ for, in this case, mesh surface data. All of these have $h/\delta \approx 0.06$ except for the first ($Re_\theta = 954$), for which $h/\delta = 0.18$. For this case, measurements could not be made deep into the log-law region (which CC showed extends all the way down to the top of the roughness elements provided spatially averaged data are used); the figure shows the lower limit of the data and the top of the roughness in this case ($h/\delta = 0.18$). The results are also independent of θ/y_o, the parameter which controls the surface friction, C_f, defined in the usual way. Very similar data were obtained over the other two surfaces, even extending to rather higher h/δ, as shown in Fig. 4c for the block surface roughness, where collapse is good up to at east $h/\delta = 0.18$. However, the highest h/δ data in Fig. 4c does show a noticeable (upward) shift from the regular deficit profile. This is not surprising; there is little reason to suppose that when there is hardly any classical inner region, the outer region should conform to the usual profile.

A reasonably sensitive check on the profile character is provided by Clauser's G parameter $\left((H-1)/H/\sqrt{C_f/2}\right)$, and this is plotted in Fig. 5 for the three different surfaces, along with the CC data. Coles (1987) smooth-wall value is 6.2, and the data first appear to rise from values reasonably consistent with that to a value around $G = 7$; $G = 7.03$ is the value implied by the classical two-parameter profile family with wake strength $\Pi = 0.7$ (see discussion in Castro 2007). However, as h/δ increases, there seems to be a trend of decreasing G and there is a hint that this starts rather earlier for the random block roughness than it does for either the mesh or the staggered cubes surface. h for the random block surface has been taken (throughout this paper) as the average block height; recognizing that the surface drag is dominated relatively more by the higher blocks, one could argue that a rather larger normalizing height might be appropriate in that case and this would reduce the h/δ at which the profile shape deviates from the norm. A fall in G would imply a fall in Π, but only on the assumption that the classical wake profile is maintained.

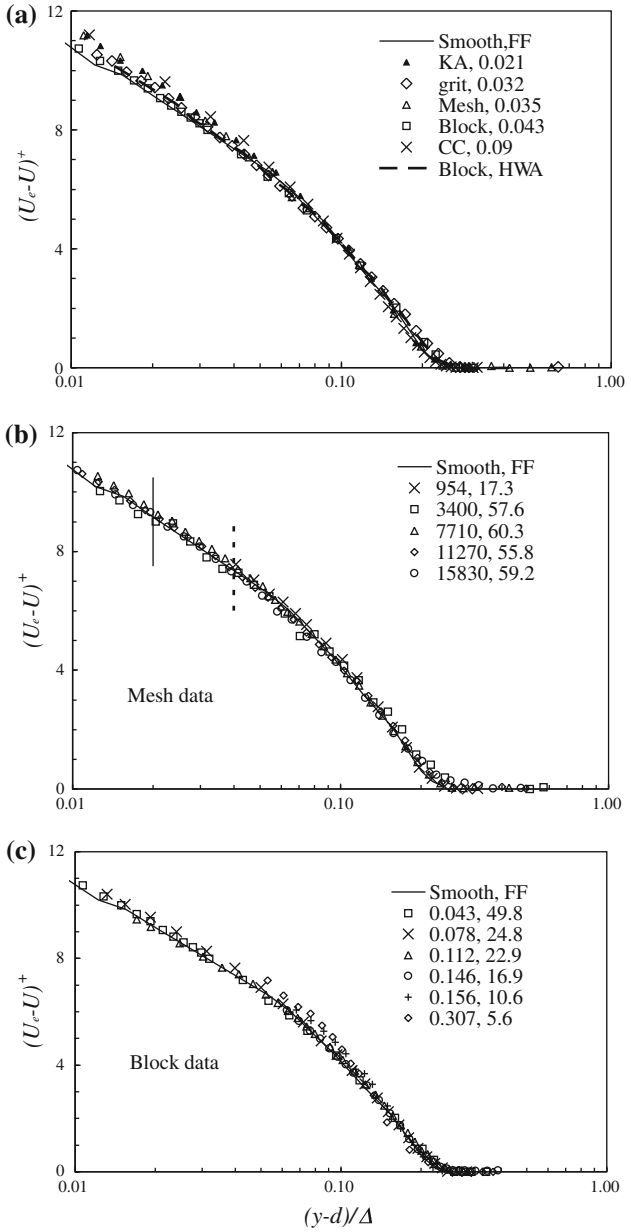

Fig. 4 **a** Mean velocity defect profiles for $Re_\theta \approx 11{,}000$, all surfaces. Legend and symbols as in Fig. 3 and Table 1. **b** mesh deficit profiles data for $h/\delta \approx 0.06$. *Numbers* in legend refer to values of Re_θ and θ/y_o. *Vertical dashed* and *solid lines* indicates lowest measurement point and the top of the roughness, respectively, for the $Re_\theta = 954$ case. **c** block deficit profiles for various h/δ, θ/y_o (values shown in legend)

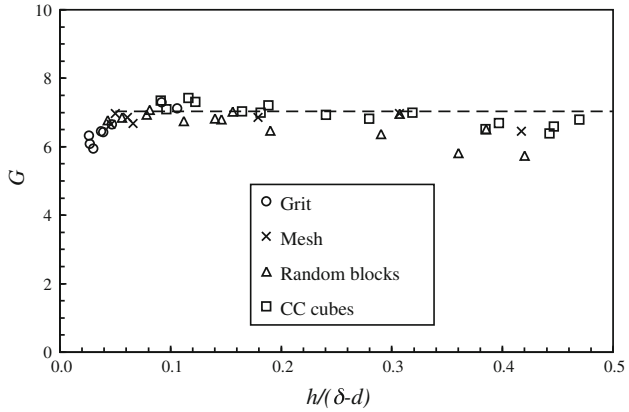

Fig. 5 The Clauser parameter as a function of y/δ. The *horizontal dashed line* is $G = 7.03$

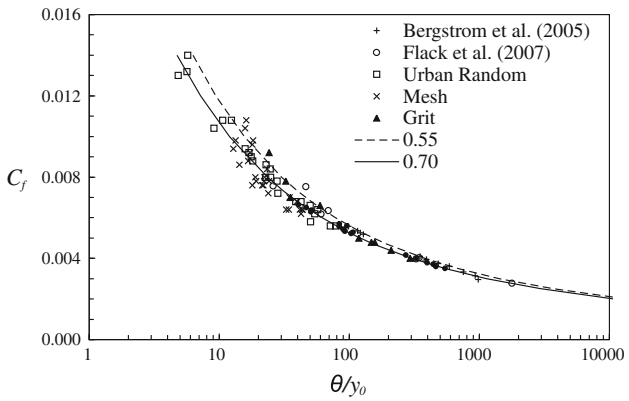

Fig. 6 The variation of C_f for all three surfaces. *Lines* refer to the standard two-parameter family result, with wake strengths of $\Pi = 0.55$ and 0.7

However, the data (not shown) do not suggest any noticeable fall in Π once $h/\delta > 0.2$, say, and are in that sense consistent with our earlier data (Castro 2007), so we conclude that the profile shape *does* change—as suggested by the $h/\delta = 0.307$ profile shown in Fig. 4c, for example.

Figure 6 shows the C_f variation for all surfaces, with the (small h/δ) data of Flack et al. (2007) and Bergstrom et al. (2005) included. The classical two-parameter mean flow result, formulated in terms of C_f vs. θ/y_o (Castro 2007), is included for two values of Π. The scatter becomes relatively large at small values of θ/y_o. This is partly because of the greater difficulty in determining both u_τ and y_o when h/δ exceeds around 0.2. However, it is known that at such large values of h/δ, there are significant spanwise variations in the boundary layer. These have been documented for block-type rough surfaces by Reynolds et al. (2007) and, in principle, would require full spanwise averaging of all quantities before truly representative mean characteristics would emerge.

Nonetheless, the data generally confirm the conclusion in our earlier paper (Castro 2007) that mean flow universality occurs independently of the nature of the surface up to quite large h/δ—perhaps up to $h/\delta = 0.2$ but certainly significantly larger than the Jiménez (2004) criterion of just a few percent. Beyond that point, there is some (albeit weak) evidence that the $(h/\delta)_c$ denoting departure from universality may be dependent on the nature of the surface.

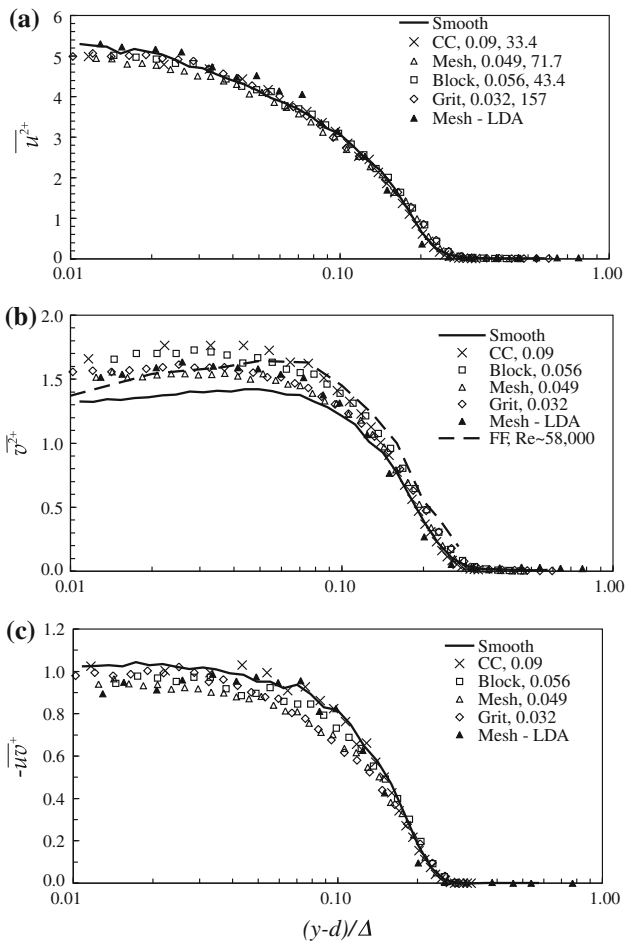

Fig. 7 Turbulence Reynolds stresses for different surfaces at various h/δ. Numbers in the legend, which describes all three figures, refer to the values of h/δ and the corresponding θ/y_o

The fact that mean flow universality extends up to $h/\delta \approx 0.2$ does not necessarily imply that turbulence statistics will similarly be universal; it is these which are the focus of this paper and which we now consider.

5 Reynolds stresses

Figure 7 shows selected normalized Reynolds stresses for all surfaces at moderate h/δ. (Re_θ lies between 6,900 and 12,600.) Our own smooth-wall data (obtained at $Re_\theta =$ 7,000) are used for comparison rather than the Fernholz and Finley (1996) data because the smooth-wall normal vertical stresses are very Reynolds number dependent. At $(y-d)/\Delta = 0.04$, for example, they reported values of $\overline{v^2}^+ = 1.18$ and 1.56 at $Re_\theta = 5{,}000$ and 58,000, respectively, compared with Erm and Joubert's (1991) value of 1.10 at $Re_\theta = 2{,}800$. The smooth-wall data in Fig. 7b ($Re_\theta = 7{,}000$) have $\overline{v^2}^+ = 1.4$ at $(y-d)/\Delta = 0.04$.

CC's data are included in the figures and good collapse in the $\overline{u^2}^+$ data is seen (Fig. 7a), in both inner and outer regions of the boundary layer, for a factor of three range in h/δ—from 0.03 to 0.09. Similarity in the streamwise Reynolds stress for rough and smooth walls in the outer flow is well known, at least at low values of h/δ, having been observed in a number of previous studies—e.g. Raupach et al. (1991), Flack et al. (2005) and Schultz and Flack (2007). On the other hand, Krogstad et al. (1992) reported considerable (rough wall) modifications in the inner layer and discernable differences even in the outer layer. The reason for these differences, which do not appear in the present data, is unclear. It is also worth emphasizing that the mesh data show no sign of departure from the usual inner layer behaviour, either in the defect velocity (Fig. 4) or in the streamwise stress (Fig. 7a). This is in distinct contrast to the data over the identical mesh but in a channel flow, recently presented by Birch and Morrison (2010), with $h/\delta = 0.078$ where here δ is the channel half-depth. However, they used a single hot wire parallel to the surface. It is possible that, given the high-turbulence intensities once $(y-d)/\Delta < 0.1$, the data were contaminated by the vertical fluctuating velocity component, which would have the effect of increasing the mean axial velocity and reducing the axial Reynolds stress, as seen in their data. Our 120° cross wire and LDA probes avoid this difficulty. Note that the LDA data, included in the figure for the particular mesh case shown, agree reasonably with the corresponding HWA data, except in the very-near-wall region where differences are not perhaps insignificant. The reasons are not clear, other than the usual uncertainties in u_τ and experimental errors in high-turbulence regions. If the LDA near-wall $-\overline{uv}$ point had been used, rather than the peak, to deduce u_τ, the LDA $\overline{v^2}^+$ data would generally be rather closer to the HWA data, but the agreement in $\overline{u^2}^+$ would be less satisfactory.

There is a reasonable collapse in all the $\overline{uv}^+$ data (Fig. 7c), at least within the likely experimental uncertainties. However, the normal stress data shown in Fig. 7b clearly do not collapse and all lie, to various extents, significantly above the smooth-wall result at similar Re_θ, at least within the inner region. The large outer layer differences noted by Krogstad et al. (1992) are not evident, although there are perhaps small increases above the smooth-wall profile. There is a suggestion that in the inner region, the increases above the smooth-wall profile are larger for larger h/δ, a point to which we return later. Fig. 7b includes the very-high-Reynolds number smooth-wall data reported by Fernholz and Finley (1996)—for $Re_\theta \approx 58{,}000$. Given the independence of the fully rough profiles on Re_θ (see below), one could argue that, at least in the outer flow, the data should be comparable with these

high-Reynolds number smooth-wall results. There is little discernable trend in the rough-wall data in the outer region, and they all lie between the low- and high-Reynolds number smooth-wall data. In the inner region, however, it is clear that profiles from the largest h/δ cases shown are higher than both smooth-wall profiles.

Figure 8 shows typical $\overline{v^2}^+$ profiles at various values of h/δ for the grit surface. It presents data from the lowest and highest h/δ sets and includes the smooth-wall profiles reported by Fernholz & Finley at low and high Re_θ as well as the present smooth-wall data. Within experimental uncertainty, there is good collapse of all the mesh data for this surface, with no trend between the low and high h/δ cases. It is perhaps again significant that, as for the mesh data in Fig. 7b, the rough-wall results lie close to those reported for smooth walls at very high Re_θ. It is worth emphasizing that the rough-wall stress data are not dependent on Reynolds number. There is a factor of two variation in Re_θ in the data shown in Fig. 7b but this cannot explain the small trend (which, as noted above, follows the variation of h/δ); for example, both the grit data and the block data have Re_θ values almost twice that of the mesh data. Likewise, the grit data shown in Fig. 8 cover the range $1{,}100 < Re_\theta < 11{,}000$ with no discernible trend in the profiles. Careful scrutiny of our full set of profiles reveals no obvious trends with Re_θ in any parameter, and it seems that Re_θ is simply not a governing parameter (as argued for the mean flow in Castro 2007). Neither, at least for this range of h/δ, is θ/y_o. (Recall that the latter replaces Re_θ as the parameter which determines the skin friction for fully rough boundary layers, see Fig. 6.) For the grit surface, the degree of collapse for both $\overline{u^2}^+$ and $-\overline{uv}^+$ is at least as good as that seen for $\overline{v^2}^+$ (so the data are not shown here), although for the two higher h/δ cases, the peak $\overline{u^2}^+$ in the inner region was noticeably lower than it was for smaller h/δ (see below). Note that for this (grit) surface, it was not possible to obtain data for h/δ greater than about 0.15, for that would have required measurements very near the leading edge of the rough surface, where the boundary layer is relatively thin and may not have recovered from leading edge effects.

Block roughness data are shown in Fig. 9. Note first that for small h/δ (below about 6%), the $\overline{u^2}$ and $-\overline{uv}$ data lie close to the smooth wall results throughout the boundary layer, as seen earlier, whereas the $\overline{v^2}$ data are similar to the high-Re_θ smooth-wall profile. This is all consistent with results for the other two surfaces for relatively low h/δ. As h/δ rises, however, although in the outer region the $\overline{u^2}$ still collapse, there are significant falls in the peak values

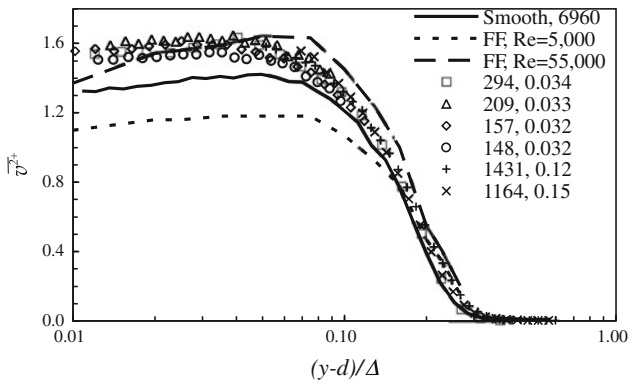

Fig. 8 Vertical normal stress profiles at various h/δ for the grit surface. *Numbers* in the legend refer θ/y_o and h/δ. *Solid line* refers to the present smooth-wall data at the Re_θ shown; *dotted* and *dashed lines* refer to the Fernholz and Finley (1996) profiles at $Re_\theta \approx 5{,}000$ and 55,000, respectively

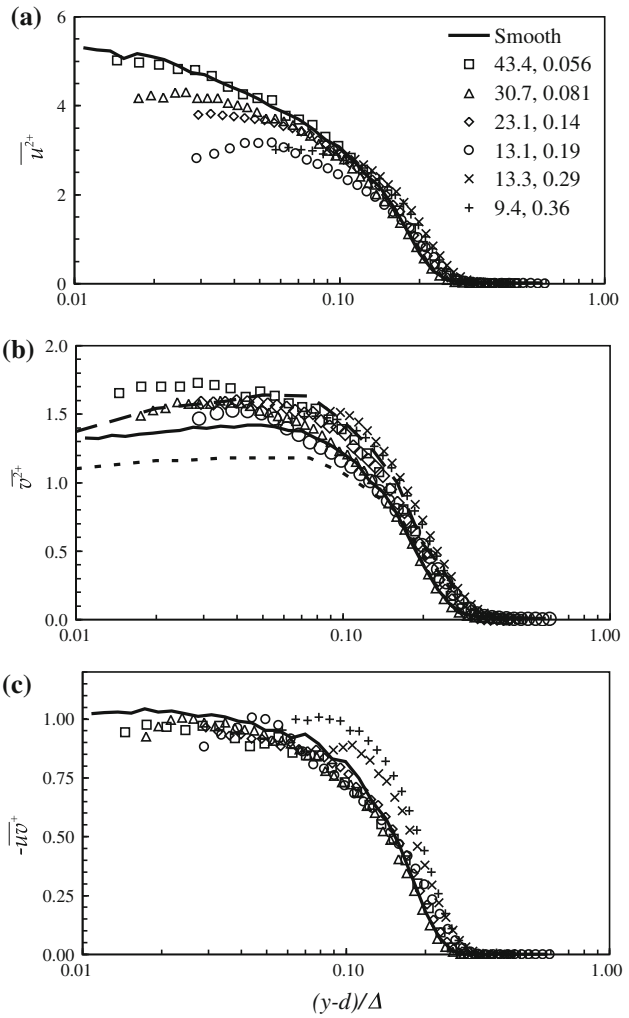

Fig. 9 Stress profiles at various h/δ for the block surface. *Numbers* in the legend refer θ/y_o and h/δ. *Solid line* refers to the present smooth-wall data at $Re_\theta = 6960$; *dotted* and *dashed lines* refer to the Fernholz and Finley (1996) profiles at $Re_\theta \approx 5{,}000$ and 55,000, respectively

reached in the inner region, as mentioned above for the grit data. Of course, for high h/δ, it is less easy to determine precise values of u_τ, but the trend in Fig. 9a is obvious. On the other hand, in the inner region, there is no clear trend in the $\overline{v^2}$ data shown in Fig. 9b. What seems more clear, however, is that outer region data become increasingly affected as h/δ rises above about 0.2. This is particularly evident in the shear stress profiles (Fig. 9c). It is not surprising; for any given surface, there must exist an $(h/\delta)_c$ beyond which not only the inner region but also the outer region must be affected by the roughness, as argued earlier. Indeed, what is likely, and indeed is suggested by these data, is that the turbulence characteristics in the usual inner region change entirely—in fact, the inner region must eventually disappear, which has implications for the mean velocity profile. Once h/δ approaches $(h/\delta)_c$, there is usually insufficient data in the near-wall region to identify a genuine log-law region; given too the possible uncertainty in the value of κ, the von Kármán constant, for such surfaces (see Leonardi and Castro 2010, for a recent discussion of this point), obtaining a unique set of d, y_o, u_τ and κ by assuming the existence of a log-law region is not possible. This is the major reason for the scatter at low θ/y_o in Fig. 6. Such flows should arguably be considered as shear flows over groups of obstacles, rather than genuine boundary layers in the classical sense, as Jiménez (2004) implied.

A relatively sensitive test to assess the effect of the surface on the Reynolds stresses is to plot the structural parameter $\overline{v^2}/\overline{u^2}$, which does not rely on sometimes uncertain values of u_τ. This is done in Fig. 10 for a location in the inner region defined by $(y-d)/\Delta = 0.04$. Recent LDA data for the CC case (Hayden, personal communication) are included as are the low and high Re_θ values reported by Fernholz and Finley (1996). There is no evidence of any significant trend in the data for h/δ below about 0.2, although the block surface data might perhaps suggest the earliest rise above the smooth-wall value, which would be consistent with the earlier change in mean flow profile noted in Sect. 4. However, $\overline{v^2}/\overline{u^2}$ rises significantly with h/δ larger than about 0.2. For low values of the latter, one might expect θ/y_o to be more important than h/δ, and Fig. 10b shows the data plotted against the former. (Note that large h/δ corresponds to small θ/y_o.) However, above the inevitable scatter caused by summation of errors in $\overline{v^2}$ and $\overline{u^2}$, there is no apparent trend for $\theta/y_o > 20-30$. Around $\theta/y_o = 10$, however, there are large variations. Some of these are undoubtedly due to the effects of initial conditions at small fetches. An alternative set of CC experiments was undertaken with the leading edge ramp rising to the top, rather than the bottom, of the roughness elements; the data are included in the figure, and it is clear that there are significant differences for $\theta/y_o = 10-20$ (Fig. 10b). For these short fetches and consequent very large h/δ, the latter is arguably a more appropriate scaling parameter, because θ is very dependent on the shape of the mean velocity profile. Figure 10a certainly shows a rather better collapse of the data with h/δ once this exceeds about 0.2 ($\theta/y_o < 15$, say). Very similar results are apparent in the outer layer; the data do not differ much in form from those shown in Fig. 10, although for $h/\delta < 0.2$ $\overline{v^2}/\overline{u^2}$ lies between the low- and high-Reynolds number smooth-wall values. This is illustrated in Fig. 11, which shows data at $(y-d)/\Delta = 0.15$—i.e. around the central region of the boundary layer ($y/\delta \approx 0.5$). Comparison of Figs. 10a and 11 suggests that the rise above the smooth-wall value begins rather later in the outer region, which is what one would expect. Turbulence structural changes occur first near the surface but extend gradually into the outer flow as the relative roughness height increases. This is explored further in the following section.

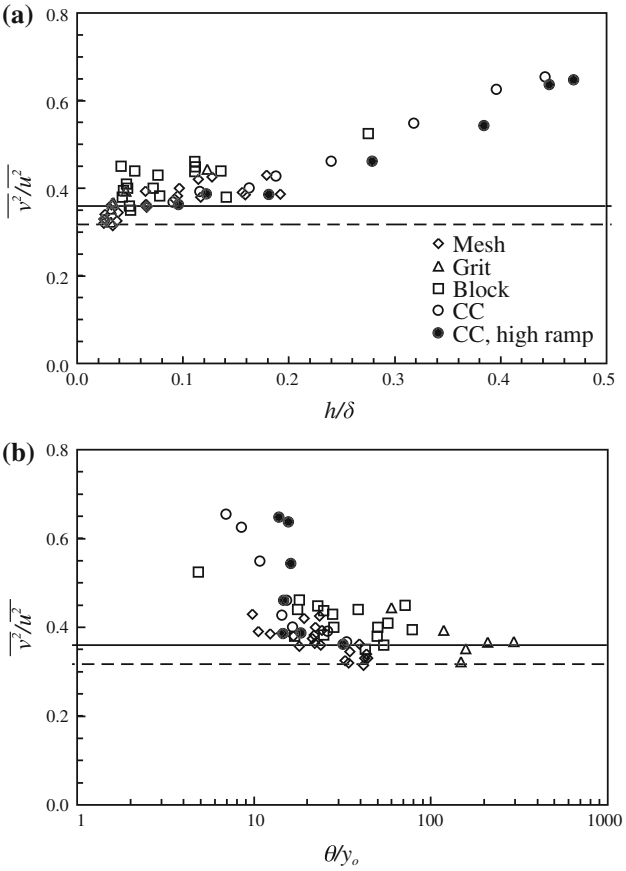

Fig. 10 $\overline{v^2}/\overline{u^2}$ at $y/\Delta = 0.04$ as a function of h/δ, (**a**), and θ/y_o, (**b**). *Dashed* and *solid lines* are respectively the low- and high-Reynolds number smooth-wall data from Fernholz and Finley (1996)

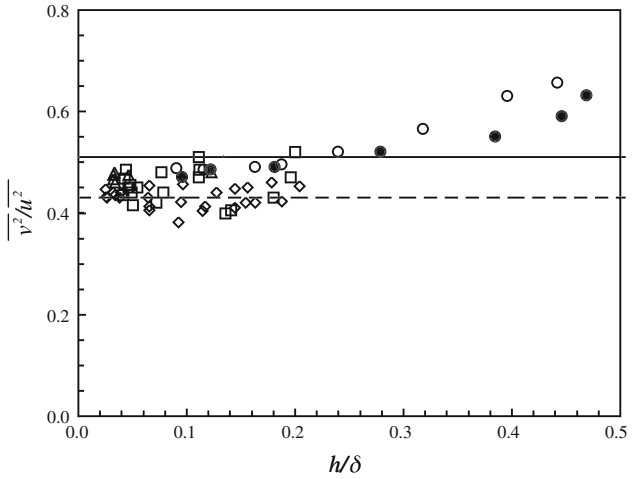

Fig. 11 $\overline{v^2}/\overline{u^2}$ as a function of h/δ at $(y-d)/\Delta = 0.15$. *Dashed* and *solid lines* are as in Fig. 10

6 Quadrant analysis

Quadrant analysis was first introduced over 40 years ago and allows one to investigate the strongest Reynolds-stress-producing events in turbulent flows. This method decomposes the mean Reynolds shear stress $\overline{uv}$ into four distinct Reynolds-stress-producing events based on the quadrant Q in the uv plane in which they reside. These events include outward interactions ($Q1$: $u > 0$, $v > 0$), ejections ($Q2$: $u < 0$, $v > 0$), inward interactions ($Q3$: $u < 0$, $v < 0$) and sweeps ($Q4$: $u > 0$, $v < 0$). This methodology has been used extensively to study the Reynolds-stress-producing events in turbulent boundary layers as well as turbulent channel and pipe flows. One of the first major discoveries (Wallace et al. 1972) was that in the wall region above a smooth surface one ejections and sweeps represent the dominant Reynolds-stress-producing events, with each contributing nearly 70% to the total Reynolds stress at $y^+ \approx 15$, whereas inward and outward interactions each yielded 20% contributions. Below $y^+ \approx 15$, the sweeps and outward interactions were more dominant. It seems that most of the Reynolds stress is generated by the large, energetic motions (Wallace and Brodkey 1977).

Grass (1971) was perhaps the first to use the technique for a rough-surface flow; he investigated intermittent ejections and sweeps in rough-wall boundary layers using hydrogen bubble visualization and found that the entrainment of low momentum fluid trapped between the roughness elements was much more violent than the entrainment of the smooth-wall viscous sublayer fluid. Raupach (1981) observed that sweeps accounted for most of the turbulent stress near rough surfaces and that the relative magnitude of the sweep component increased both with surface roughness and with proximity to the surface, mirroring in general terms what happens below $y^+ \approx 15$ above a smooth surface. Likewise, Krogstad et al. (1992) observed that contributions from sweeps are significantly greater over a rough surface (wire mesh) than over a smooth surface, particularly in the near-wall region. They also found that strong ejections and sweeps occurred almost twice as frequently in the presence of surface roughness.

In the present study, a quadrant analysis using the method of Lu and Willmarth (1973) was performed. Using the concept of a hyperbolic hole of size H, defined by $|uv| = Hu'v'$ where primed quantities denote rms values, a detector indicator function, $I_Q(t)$, was defined so that

$$I_Q(t) = \begin{cases} 1 & \text{if } |uv|_Q \geq Hu'v' \\ 0 & \text{otherwise} \end{cases} \tag{4}$$

where Q denotes the quadrant of interest. The contribution to $\overline{uv}^+$ from a particular quadrant may be written as

$$(\overline{uv})_Q = \frac{1}{T}\int_0^T uvI_Q(t)dt. \tag{5}$$

Detections were made using a range of values for the threshold level H, although results are presented here only for $H = 2.5$, corresponding to events which are associated with $uv > 6\overline{uv}$. All the data presented in this section were acquired using HWA.

Figure 12 shows the percentages of the total shear stress provided by the strong ($H = 2.5$) $Q2$ ejection events and $Q4$ sweep events. The data were obtained at the most downstream fetch position for each roughness, so that the values of h/δ were small in each case. Data for the smooth wall are also shown. Ejection events clearly dominate sweeps throughout the boundary layer for the smooth wall and also for the rough surfaces provided $y/\Delta > 0.025$. There is good agreement among all surfaces across almost the entire boundary layer. However, noticeable differences are observed in the near-wall region. Very near the smooth wall, the contribution of strong $Q2$ events is more pronounced than on the rough walls. The rise in the contribution from strong $Q2$ ejection events on smooth walls was also documented by Krogstad et al. (1992). On the rough wall, in contrast, the strong $Q4$ events (Fig. 12b) are enhanced for $y/\delta < 0.05$. This is illustrated more clearly in Fig. 12c, which shows the ratio of the contributions from $Q2$ and $Q4$ for $H = 2.5$. It can be seen that the ratio is less than unity for the mesh and block surfaces below about $y/\Delta = 0.02$ but greater than unity for the smooth wall. This indicates that whilst strong ejection events play a relatively larger role near a smooth wall, sweeps have a larger contribution near rough walls. Such behaviour was also observed by Raupach et al. (1981) and Krogstad et al. (1992) and the latter speculated that it is probably a result

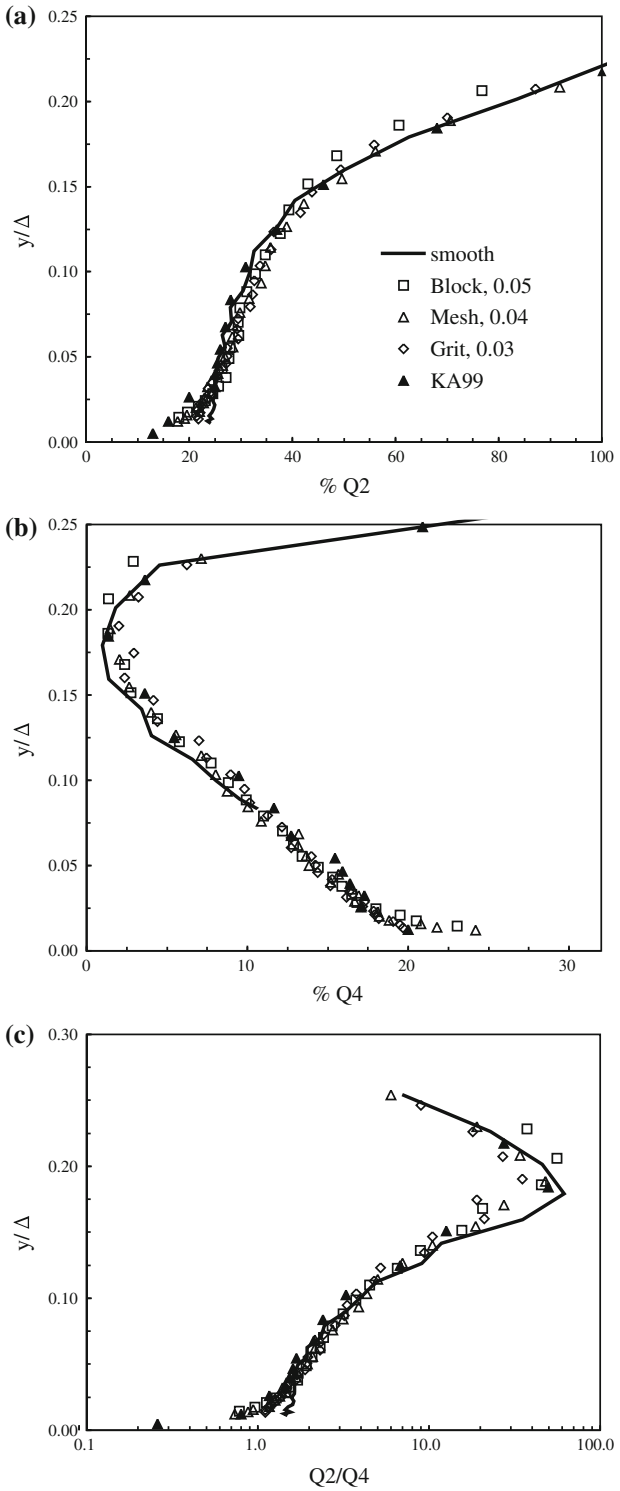

Fig. 12 Percentage contributions to $-\overline{uv}$ for $H = 2.5$ from **a** $Q2$ (ejections) and **b** $Q4$ (sweeps) for all surfaces with small h/δ. Values of the latter are given in the legend. **c** Ratio of shear stress contributions from $Q2$ and $Q4$ for $H = 2.5$

of the 'less solid' boundary condition for wall-normal flow near the top of the roughness. The more recent results of Krogstad and Antonia (1999) are included in the figure, and the present results for both the $Q2$ and $Q4$ events are in good agreement with their mesh surface data. Flack et al. (2005) also showed good agreement for both the $Q2$ and $Q4$ contributions outside the near-wall region between their smooth, sandpaper and mesh surfaces.

Once h/δ rises above a few percent, differences in these structural parameters become noticeable further away from the wall. This is illustrated using the block surface data in Fig. 13. As h/δ increases the strong ejection events in the near-wall region become increasingly suppressed, whilst strong sweeps become more significant. The figure includes data from Reynolds and Castro (2008) for a surface comprising an array of staggered cubes (identical to the CC surface), at $h/\delta = 0.074$. These data have the same overall behaviour of reductions in $Q2$ and increases in $Q4$ contributions near the wall, but significant differences from the present data are evident below about $y/\Delta = 0.05$. However, this profile was obtained at a specific (x, z) location (actually above the centre of a cube) and since the roughness sublayer extended to around that value of y/Δ, the results are very dependent on the specific location chosen. Recall that in the present work, block roughness profiles were deliberately obtained at a location where the velocity and turbulence stresses, for example, happened to be about the same as the full spatial averages.

Away from the wall, beyond about $y/\Delta = 0.07$, there is a reasonable collapse in all the rough-wall data with the smooth wall results provided the roughness height does not exceed about $y/\delta = 0.13$. It is clear that as h/δ rises, the near-wall changes increasingly encroach into the outer region. Results for the mesh surface follow the trends of both the grit and block roughnesses for equivalent h/δ values. It is difficult to discern any clear indication that the nature of, for example, the sweep/ejection contributions to the shear stress for any given h/δ are dependent on the nature of the surface.

7 Final discussion and conclusions

The data presented in this paper show that zero-pressure gradient rough-wall boundary layers are indistinguishable from smooth-wall flows, independently of the nature of the roughness provided that its height does not exceed about 15% of the boundary layer thickness. In particular, the mean velocity profiles conform to the classical two-parameter family, although the wake strength rises to values around 0.7 from the Coles smooth-wall value (0.62) so that the Clauser parameter rises to about 7. This is consistent with our earlier findings for an even wider range of (3D) roughnesses (Castro 2007). Turbulence stresses are also consistent with the highest Reynolds number smooth-wall data available, both throughout the outer layer and in

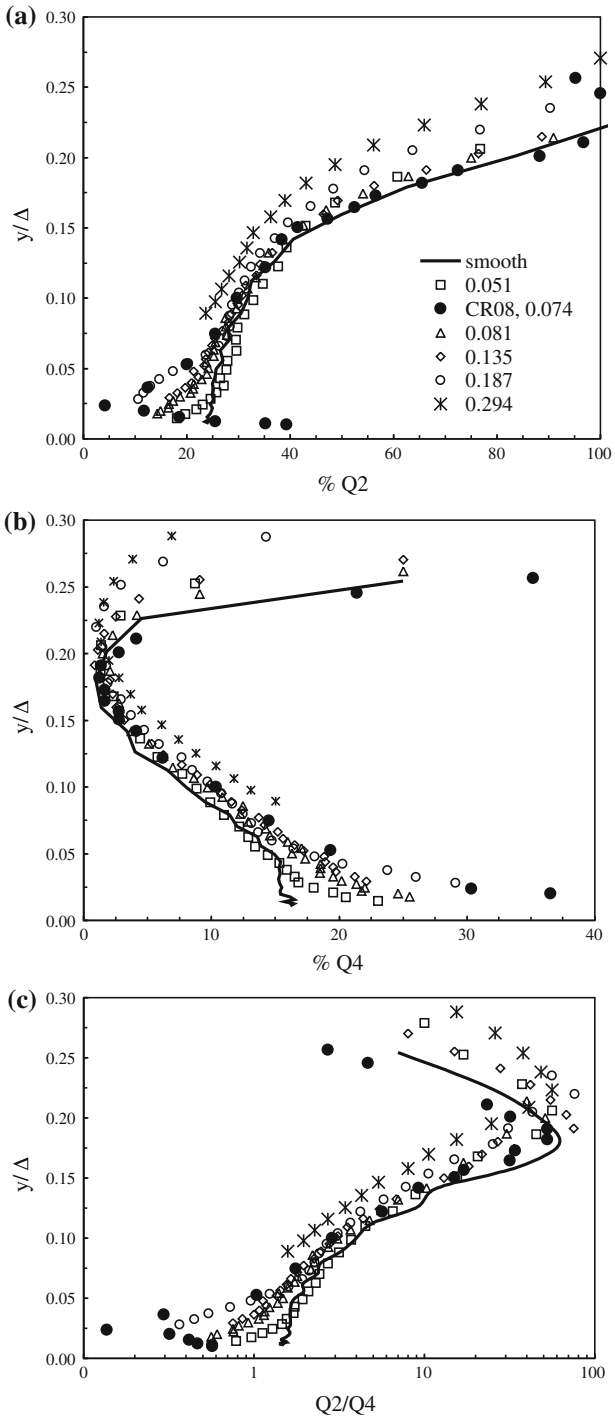

Fig. 13 Percentage contributions to $-\overline{uv}$ for $H = 2.5$ from **a** $Q2$ (ejections) and **b** $Q4$ (sweeps) for block roughness at various h/δ. Values of the latter are given in the legend. **c** Ratio of shear stress contributions from $Q2$ and $Q4$ for $H = 2.5$; *filled cricle* data from Reynolds and Castro (2008) for staggered cube roughness

the inner layer, down to the spatially inhomogeneous region synonymous with the roughness sublayer. Likewise, quadrant analysis suggests that the detailed structure of the turbulence is unaffected in the outer layer by either the nature of the roughness or its size, provided that h/δ is below about 15%. We argue that in view of all this, a rough-wall boundary layer is equivalent in many ways to a very-high-Reynolds number smooth-wall boundary layer, except of course for the enhanced skin friction. For three-dimensional roughness of any type, we suggest that the critical roughness height below which Townsend's hypothesis remains valid is around $(h/\delta)_c = 0.15$.

In view of some extant data on two-dimensional (bar) roughness, this conclusion may hold only for genuinely three-dimensional roughness. Krogstad and Antonia (1999) and, more recently, Schultz et al. (2010) have found that 2D bar roughness can lead to significant changes in outer layer stresses even for quite small values of h/δ—0.031 in the latter case, for example. Schultz et al. showed that the enhanced stresses were due to large-scale turbulent motions emanating from the wall and argued that whilst for 3D roughness the largest scale motions generated by the roughness itself have a size of O(h), 2D bars may produce much larger scale motions. In the 3D case, our data, like those of earlier authors, show structural changes within the inner layer even for small roughness. These are typified by stronger Q4 events, probably arising because the damping of $\overline{v^2}$ provided by a rough wall is weaker than it is for a smooth flow (Krogstad et al. 1999). However, these structural changes do not appear to have a significant influence on first- and second-moment data (i.e. mean velocity and Reynolds stresses).

Note that much of this is in contrast to what is found in 2D channels, where the evidence is that neither quite large 3D roughness (Leonardi and Castro 2010) nor 2D bar roughness (Krogstad et al. 2005) affects the outer layer turbulence. This must be a result (partly at least) of the much 'harder' outer boundary condition for internal flows.

Our data also display evidence that once h/δ exceeds about 0.15, not only the mean flow profile but also the turbulence begins to be affected in the outer layer. And there are hints that the point at which this begins depends somewhat on the nature of the roughness. Although the evidence for this is weak, it does not seem unlikely since eventually, as Jiménez (2004) pointed out, the flow becomes essentially flow over a collection of obstacles, rather than a boundary layer as usually understood. Certainly, by the time $h/\delta = 0.3$ changes extend throughout all the outer layer and even the mean velocity profile is noticeably affected. For such flows, the usual paradigms for near-wall modelling (and scaling) are probably not appropriate, and the flow over any specific surface has to be treated as an individual case, likely to be different in many ways from other cases.

Acknowledgments The authors are grateful to the UK's Engineering & Physical Sciences Research Council, who provided funding

for this work under grant number EP/D036771, and to staff in the School of Engineering Sciences' workshop, who provided willing and excellent technical support throughout the experimental programme. We also thank Paul Hayden of the University of Surrey for his valuable support with the EnFlo software used for all our data collection and Karen Flack, Per-Åge Krogstad, Jonathan Morrison and David Birch for helpful discussions.

References

Bergstrom DJ, Akinlade OG, Tachie MF (2005) Skin friction correlation for smooth and rough wall turbulent boundary layers. ASME J Fluids Eng 127:1146–1153

Bhaganagar K, Kim J, Coleman GN (2004) Effect of roughness on wall-bounded turbulence. Flow Turb Comb 72:463–492

Birch DM, Morrison JF (2010) Similarity of the streamwise velocity component in very-rough-wall channel flow. J Fluid Mech 668:174–201

Castro IP (2007) Rough-wall boundary layers: mean flow universality. J Fluid Mech 585:469–485

Cheng H, Castro IP (2002) Near-wall flow over urban-type roughness. Boundary Layer Meteorol 104:229–259

Coles DE (1987) Coherent structures in turbulent boundary layers. In: Meier HU, Bradshaw P (eds) Perspectives in turbulence studies. Springer, Berlin, pp 93–114

Connelly JS, Schultz MP, Flack KA (2006) Velocity defect scaling for turbulent boundary layers with a range of relative roughness. Exp Fluids 40:188–195

Erm LP, Joubert PN (1991) Low Reynolds number turbulent boundary layers. J Fluid Mech 230:1–44

Fernholz HH, Finley PJ (1996) The incompressible zero-pressure gradient turbulent boundary layer: an assessment of the data. Prog Aerosp Sci 32:245–311

Flack KA, Schultz MP, Connelly JS (2007) Examination of critical roughness height for outer layer similarity. Phys Fluids 19:095104

Flack KA, Schultz MP, Shapiro TA (2005) Experimental support for Townsend's Reynolds number similarity hypothesis on rough walls. Phys Fluids 17:035102

Grass AJ (1971) Statistical features of turbulent flow over smooth and rough boundaries. J Fluid Mech 50:233–255

Kline SJ, Reynolds WC, Schraub FA, Rundstadler PW (1967) The structure of turbulent boundary layers. J Fluid Mech 30:741–773

Krogstad P-A, Antonia RA, Browne LWB (1992) Comparison between rough- and smooth-wall turbulent boundary layers. J Fluid Mech 245:599–617

Krogstad P-A, Antonia R (1999) Surface roughness effects in turbulent boundary layers. Exp Fluids 27:450–460

Krogstad P-A, Andersson HI, Bakkem OM, Ashrafian A (2005) An experimental and numerical study of channel flow with rough walls. J Fluid Mech 530:327–352

Kunkel GJ, Marusic I (2006) Study of the near-wall turbulent region of the high Reynolds number boundary layer using an atmospheric flow. J Fluid Mech 548:375–402

Jackson PS (1981) On the displacement height in the logarithmic velocity profile. J Fluid Mech 111:15–25

Jiménez J (2004) Turbulent flows over rough walls. Ann Rev Fluid Mech 36:173–196

Leonardi S, Castro IP (2010) Channel flow over large cube roughness: a direct numerical simulation study. J Fluid Mech 651:519–539

Leonardi S, Orlandi P, Smalley RJ, Djenidi L, Antonia RA (2003) Direct numerical simulations of turbulent channel flow with transverse square bars on one wall. J Fluid Mech 491:229–238

Lu SS, Willmarth WW (1973) Measurements of the structure of the Reynolds stress in a turbulent boundary layer. J Fluid Mech 60:481–511

Perry AE, Li JD (1990) Experimental support for the attached eddy hypothesis in zero-pressure gradient turbulent boundary layers. J Fluid Mech 218:405–438

Perry AE, Lim KL, Henbest SM (1987) An experimental study of the turbulence structure in smooth and wough wall turbulent boundary layers. J Fluid Mech 177:437–466

Raupach MR (1981) Conditional statistics of Reynolds stress in rough-wall and smooth-wall turbulent boundary layers. J Fluid Mech 108:362–382

Raupach MR, Antonia RA, Rajagopalan S (1991) Rough-wall turbulent boundary layers. Appl Mech Rev 44:1–25

Reynolds RT, Hayden P, Castro IP, Robins AG (2007) Spanwise variations in nominally two-dimensional rough-wall boundary layers. Exp Fluids 42:311–320

Reynolds RT, Castro IP (2008) Measurements in an urban-type boundary layer. Exp Fluids 45:141–156

Rotta JC (1962) The calculation of the turbulent boundary layer. Prog Aeronaut Sci 2:1–219

Schultz MS, Flack K (2007) The rough-wall turbulent boundary layer from the hydraulically smooth to the fully rough regime. J Fluid Mech 580:381–405

Schultz MP, Volino RJ, Flack KA (2010) Boundary layer structure over a two-dimensional rough wall. In: Nickels T (ed) Proc. of IUTAM symposium on the physics of flow over rough walls. Springer

Tachie MF, Bergstrom DJ, Balachandar R (2000) Rough wall turbulent boundary layers in shallow open channel flow. J Fluids Eng 122:533–541

Tutu N, Chevray R (1975) Cross-wire anemometry in high-intensity turbulence. J Fluid Mech 71:785–800

Townsend AA (1976) The structure of turbulent shear flow, 2nd ed. CUP, p 429

Volino RJ, Schultz MP, Flack KA (2009) Turbulence structure in a boundary layer with two-dimensional roughness. J Fluid Mech 635:75–101

Wallace JM, Eckelmann H, Brodkey RS (1972) The wall region in turbulent shear flow. J Fluid Mech 54:39–48

Wallace JM, Brodkey RS (1977) Reynolds stress and joint probability density distributions in the u-v plane of a turbulent channel flow. Phys Fluids 20:251–355

Wei T, Schmidt R, McMurty P (2005) Comment on the Clauser chart method for determining the friction velocity. Exp Fluids 38:695–699